Astron. Astrophys. 337, 819–831 (1998)

ASTRONOMY AND ASTROPHYSICS

Emission line profile shapes from anisotropic resonance line scattering in planar equatorial disks

R. Ignace

Kelvin Bldg, Department of Physics and Astronomy, University of Glasgow, Glasgow G12 8QQ, Scotland, UK

Received 10 March 1998 / Accepted 12 June 1998

Abstract. The consequences of anisotropic resonance line scattering for the emission profiles of equatorial disks are considered. In particular the opportunity to infer the disk velocity field owing to the anisotropic scattering is discussed. Analytic expressions for the profile shapes are derived for the cases of constant expansion and rotation, and numerical results are given for more realistic disk velocity fields of linear expansion and Keplerian rotation. The essential result is that the anisotropic line scattering produces a different profile signature in expanding disks as compared to rotating disks, owing to the difference in the isovelocity pattern of the two cases and how the two respective patterns relate to the scattering geometry. Unlike the spherical case discussed in a preceding paper, the anisotropic effects are more significant (up to 10–20%) in disk geometries because the degree of stellar occultation depends on viewing inclination. The key to using the formulae presented here is to obtain profiles of lines that have differing degrees of anisotropic scattering. In particular, strong doublets of Lithium-like atoms (e.g., CIV 1548,1550, MgII 2796, 2803, CaII 3935, 3969 to name a few) are well-suited for comparison, with the long wavelength component scattering isotropically and the short wavelength component being partially dipole scattering. Consideration of such doublets are advantageous in that the two components arise from the same spatial location in the flow, whereas the spatial coincidence of formation for two completely different lines is not assured. Owing to several simplifying assumptions, direct application of the results presented here to observations requires somewhat restrictive conditions, yet the diagnostic potential of the method does appear promising, especially for multiplets.

Key words: line: profiles – techniques: spectroscopic – circumstellar matter – stars: early-type – stars: emission-line, Be – stars: rotation

1. Introduction

The occurrence of circumstellar disk structures ranges from the protostellar T Tauri stars (Adams et al. 1987; Kenyon & Hartmann 1987) to those of main sequence Be stars (Quirrenbach et al. 1994, 1997) to the more evolved B[e], LBV, and AGB stars (Zickgraf et al. 1985, 1986; Nota et al. 1995; Frank & Mellema 1994). A number of papers have been written on probing the structure of circumstellar disks, especially those of the Be stars, using continuum polarization (Brown & McLean 1977; Cassinelli et al. 1987; Brown & Fox 1989; Fox & Brown 1991; Fox 1991; Bjorkman & Bjorkman 1994; Wood et al. 1997), spectral energy distributions (Poeckert & Marlborough 1978; Waters 1986; Kastner & Mazzali 1989; Porter 1997), and spectral line profiles (Caroff et al. 1972; McLean 1979; Poeckert & Marlborough 1978; McKenna 1984, 1985; Jeffery 1989, 1990; Wood & Brown 1994a,b; Brown & Wood 1994; Ignace et al. 1997). Whereas most of these previous works focussed on the effects of Thomson scattering by free electrons for either the continuum polarization or the line profiles, this paper concerns how the anisotropy intrinsic to resonance line scattering may be employed to diagnose the disk structure.

The preceding paper (Ignace 1998; hereafter paper I) discussed the anisotropic line scattering in spherical winds, especially of the redshifted emission where absorption can largely be ignored. It was shown that the emission profile shape can be altered by 10% at most for realistic wind models. Although finite star depolarization (Cassinelli et al. 1987) does reduce the scattering anisotropy, the main reason why variations in the profile shapes do not exceed the 10% level is that stellar occultation blocks the scattered light from regions where the scattering anisotropy is quite prominent. However, unlike the spherical case where viewing inclination is arbitrary, interesting profile effects are expected of equatorial disks, because the significance of stellar occultation becomes a function of viewing perspective.

The fact that resonance line scattering is generally anisotropic in its angular distribution (Hamilton 1947) was discussed in paper I and references therein, so a review will not be repeated here. Suffice that the resonance scattering may be treated as a mix of isotropic and dipolar (or Rayleigh) scattering, with the parameter $E_1 \in [0, 1]$ characterizing the fraction of the total scattering that is dipolar (Chandrasekhar 1960). Hence, $E_1 = 0$ is pure isotropic scattering, whereas $E_1 = 1$ is pure dipole scattering, like that of free electrons.

As in paper I, the motivation for this study is the consequence of anisotropic line scattering in circumstellar envelopes for the emission profile. The scattering geometry relates directly to the Doppler shifted frequency at which a resonance scattered photon

Send offprint requests to: rico@astro.gla.ac.uk

will appear in the profile. Hence lines that are dipole scattering should produce rather different emission profiles from those which are isotropic scattering. An analysis of several lines with different but known E_1 values provides a new approach for constraining the flow properties of the circumstellar material. As an initial step in the consideration of equatorial disks, the discussion of this study is restricted to rather simplified cases to highlight the different features resulting from the anisotropic scattering.

In Sect. 2 the emission profile shapes are derived for optically thin planar disks in pure expansion or rotation. Initially the expansion and rotation are assumed constant leading to analytic expressions for the profile shape. Numerical profile calculations are also given for disks in linear expansion or Keplerian rotation. A discussion of the results for observations and directions for further study are given in Sect. 3.

2. Resonance line scattering in planar equatorial disks

In deriving the emission profiles from equatorial disks, several assumptions are made, as follows:

1. The intrinsic line profile is treated as a delta function in frequency.
2. The line is optically thin.
3. The disk is axisymmetric planar at the equator, hence a delta function along the symmetry axis, z_*.
4. Only pure radial expansion or rotation are treated.
5. The disk density distribution is fixed to facilitate comparison between the expansion and rotation cases.

This rather restrictive set of assumptions allows to focus on the effects of anisotropic scattering for the profile shape, in distinction to other model parameters that affect the line profile.

Now consider the general scattering of stellar light at a point $\mathbf{r}$ in an extended circumstellar envelope with number density of scatterers $n(\mathbf{r})$ and velocity field $\mathbf{v}(\mathbf{r})$. Applying the first assumption, which forms the basis for the well-known Sobolev theory (e.g., Mihalas 1978), the stellar light interacts with atoms in an isovelocity zone, so the scattering cross section becomes

$$\sigma_\nu = \sigma_l \, \delta(\nu_{\rm obs} - \nu_{\rm z}). \tag{1}$$

The factor σ_l is the frequency integrated cross section given by $\sigma_l = \lambda_{\rm ul}^2 g_{\rm u} A_{\rm ul}/8\pi g_l$, where $\lambda_{\rm ul}$ is the line wavelength of the transition u to l, $A_{\rm ul}$ is the Einstein transition probability, and $g_{\rm u}$ and g_l are the statistical weights of the upper and lower levels. The δ-function ensures that the stellar light interacts with the scattering atoms only where the observed frequency $\nu_{\rm obs}$ is equal to the Doppler shifted frequency $\nu_{\rm z}$ of the moving scatterers along the line-of-sight (see Fig. 1), as given by

$$\nu_{\rm z} = \nu_{\rm ul} \left(1 - \frac{v_{\rm z}}{c}\right). \tag{2}$$

where $v_{\rm z} = -\mathbf{v} \cdot \hat{\mathbf{z}}$ is the observed projected bulk velocity.

For the second assumption of an optically thin line, the specific flux of line *emission* observed at $\nu_{\rm obs}$ in the profile corresponding to velocity shift $v_{\rm obs}$ is given by a volume integral over the isovelocity zone, viz,

$$F_\nu = \frac{1}{D^2} \int_{v_{\rm z}} n(\mathbf{r}) \, \sigma_l \, \delta(\nu_{\rm obs} - \nu_{\rm z})$$

$$\left[J_\nu - \frac{1}{8} E_1 (3K_\nu - J_\nu)(1 - 3\sin^2 i \cos^2 \varphi)\right] p dp d\alpha dz, \tag{3}$$

where the cylindrical coordinates (p, α, z) and (R, φ, z_*) are defined in Fig. 1, J_ν and K_ν are the familiar Eddington moments of the stellar radiation field, and D is the distance to the star. The terms appearing in the brackets inside the integral result from considerations of Rayleigh scattering of the stellar intensity (see Chandrasekhar 1960; Stenflo 1994). Note that the star is taken to be of uniform brightness (i.e., no limb darkening or starspots).

The optical thinness of the line implies that every photon scattered in the circumstellar envelope will escape. The volume integral (3) may therefore be evaluated equally well in any set of coordinates, for which the most convenient is (R, φ, z_*) of the stellar system, with $p \, dp \, d\alpha \, dz = R \, dR \, d\varphi \, dz_*$. The integration in z_* is trivially solved by applying the third assumption of a planar disk:

$$\Sigma(R) = \int_{-\infty}^{\infty} n(\mathbf{r}) \, dz_*, \tag{4}$$

where Σ is the surface number density (cm^{-2}). Given the change of variable in the integration and the chosen density distribution, the line emission of Eq. (3) reduces to a surface integral

$$F_\nu = \frac{\sigma_l}{D^2} \int_{v_{\rm z}} \delta(\nu_{\rm obs} - \nu_{\rm z}) \, \varpi \, \Sigma$$

$$\left[J_\nu - \frac{1}{8} E_1 (3K_\nu - J_\nu)(1 - 3\sin^2 i \cos^2 \varphi)\right] \, d\varpi d\varphi, \tag{5}$$

where $\varpi = R/R_*$ is the normalized cylindrical radius with R_* the innermost radius of the scattering volume.

The next step is to eliminate the δ-function in frequency. To do so requires that the velocity field be specified, which for an equatorial disk is taken as $\mathbf{v} = v_{\rm R}\hat{\mathbf{r}} + v_\varphi \hat{\varphi}$. The line-of-sight Doppler shift becomes (e.g., Wood et al. 1993)

$$v_{\rm z} = -v_{\rm R} \sin i \cos \varphi + v_\varphi \sin i \sin \varphi. \tag{6}$$

The line profiles from a disk observed at inclination i will have widths in the range $[-v_{\rm max} \sin i, +v_{\rm max} \sin i]$, where $v_{\rm max} = v_\infty$ for the case of radial expansion and $v_{\rm rot}$ for the case of rotation. It is convenient to introduce the normalizations $w_{\rm z} = v_{\rm z}/v_{\rm max} \sin i$, $w_{\rm R} = v_{\rm R}/v_{\rm max}$, and $w_\varphi = v_\varphi/v_{\rm max}$, so that

$$w_{\rm z} = -w_{\rm R} \cos \varphi + w_\varphi \sin \varphi, \tag{7}$$

thus $w_{\rm z} \in [-1, +1]$. The δ-function can be eliminated using the following relation

$$\delta \left[\nu_{\rm obs} - \nu_{\rm z}(\varphi)\right] = \delta(\varphi - \varphi_0) \left|\frac{d\nu_{\rm z}}{d\varphi}\right|^{-1} \tag{8}$$

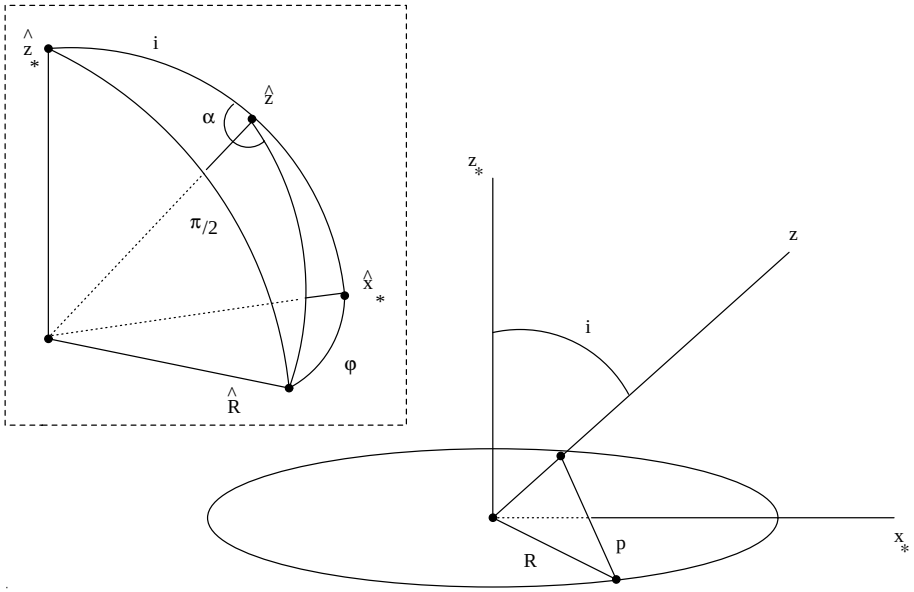

Fig. 1. Resonance line scattering in a circumstellar planar disk with surface number density $\Sigma(R)$ and velocity field $\mathbf{v}(R)$. The coordinates (p, α, z) and (R, φ, z_*) are the cylindrical coordinates of the observer and star, respectively. The angle i is the viewing inclination. The z axis is located in the $x_* - z_*$ plane.

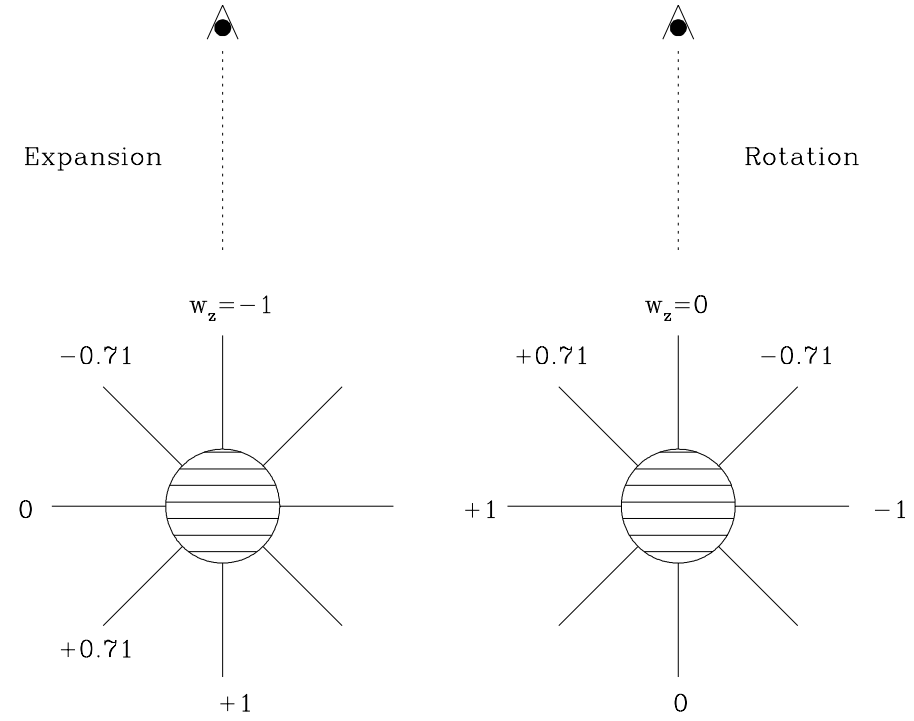

Fig. 2. Shown are two schematics of the isovelocity zones: constant expansion case on left and constant rotation case on right. The isovelocity zones are radial spokes. A few lines with labels for Doppler shifts are shown as examples.

$$= \frac{\lambda_{ul}}{v_{\max} \sin i} \delta(\varphi - \varphi_0) \, |w_{\rm R} \sin\varphi_0 + w_\varphi \cos\varphi_0|^{-1} \, . \quad (9)$$

where φ_0 represents the locus of points (i.e., the isovelocity zone) satisfying the condition that $\nu_{\rm obs} - \nu_{\rm z}(\varphi) = 0$. Substituting into Eq. (5) and evaluating the integral over azimuth gives

$$\frac{F_\nu}{F_0} = \int_{w_z} \left[\tilde{J}_\nu - \frac{1}{8} E_1 (3\tilde{K}_\nu - \tilde{J}_\nu)(1 - 3\sin^2 i \cos^2\varphi_0) \right] |w_{\rm R} \, \sin\varphi_0 + w_\varphi \, \cos\varphi_0|^{-1} \, (\Sigma/\Sigma_0) \, \varpi \, d\varpi, \quad (10)$$

which is now a line integral in ϖ over the isovelocity zone. The variable Σ_0 is a scaling parameter of the disk density so that Σ/Σ_0 is a function of ϖ only. The various constants have been collected into $F_0 = L_\nu \, \sigma_l \, R_* \, \Sigma_0 \, \lambda_{\rm ul}/8\pi \, D^2 \, v_{\max} \sin i$ and the normalized Eddington moments $\tilde{J}_\nu$ and $\tilde{K}_\nu$ are J_ν and K_ν divided by $L_*/16\pi^2 {R_*}^2$. Note that the value of F_0 will vary from line to line.

Unlike the spherically symmetric case of paper I where the inclination is arbitrary, the viewing perspective in the disk case can have major consequences for the emission profile, because the stellar occultation and the attenuation of starlight by the intervening disk are strongly dependent on inclination. The following sections consider the consequences of the anisotropic

line scattering and discuss the different aspects of finite star effects.

2.1. Line profiles from disks in constant expansion or rotation

First, only constant expansion or rotation are considered. The speed v_0 is introduced such that either $v_{\rm R} = v_0$ and $v_\varphi = 0$ or $v_{\rm R} = 0$ and $v_\varphi = v_0$. Constant expansion or rotation implies that $w_{\rm R}$ and w_φ are either 0 or 1. Thus, Eq. (7) for the Doppler shift toward the observer depends only on azimuth, and the resultant isovelocity zones are radial spokes, as shown in Fig. 2. The pattern of Doppler shifts for expansion versus rotation is shifted 90° clockwise (i.e., for stellar rotation in the counterclockwise sense).

Note that Fig. 2 may be used to infer the equivalence of the line profiles in the case of isotropic scattering by arguments of symmetry. Setting $E_1 = 0$ in Eq. (5), the specific flux of emission from a given isovelocity zone depends only on the integral of the mean intensity throughout that region. Since the arrangement of isovelocity zones for constant expansion and constant rotation are distinguished only by a rotation of the fixed pattern (i.e., all Doppler shifts in $w_{\rm z}$ between -1 and $+1$ are represented and the relative spacing of the spokes is the same because $\cos\varphi = \sin(\pi/2 - \varphi)$), the profiles must be identical, provided that finite star effects are ignored.

Furthermore, the profile shapes are expected to be double-horned (e.g., Struve 1931) based on the following argument. Considering first the case of expansion, it is well-known that an optically thin spherical shell produces a flat-topped emission profile (e.g., Menzel 1929). The emission profile of an equatorial ring can crudely be viewed as the difference between the flat-top profile of the whole spherical shell and the contribution arising from the two polar caps. The polar caps encompass a relatively large fraction of the region giving rise to low velocity emission as compared to that at high velocities, hence the profile of an equatorial ring will be severely deficient of flux near line center as compared to the line wings (Cassinelli 1998, priv. comm). It can be shown that an analogous spherical shell of uniform rotation also produces a flat-top profile, just as for uniform expansion, so that a similar line of reasoning yields a double-horned profile for the case of a rotating ring.

In the following sections, analytic expression for the emission profile from the disk are derived for anisotropic resonance scattering. Beginning first with the simple case of a point source of illumination, stellar occultation and finite star depolarization effects are included separately and together to assess the consequences of the star's finite size for the profile shape.

2.1.1. The point star approximation

Treating the star as a point source of illumination implies $\tilde{J}_\nu = \tilde{K}_\nu = \varpi^{-2}$. Taking the disk density to be $\Sigma = \Sigma_0\,\varpi^{-1}$, Eq. (10) for the specific flux in the line profile becomes

$$F_\nu \;=\; F_0\,|w_{\rm R}\,\sin\varphi + w_\varphi\,\cos\varphi|^{-1} \left[1 - \frac{1}{4}\,E_1\,(1 - 3\sin^2 i\cos^2\varphi)\right] \tag{11}$$

Since only pure expansion or pure rotation is considered, the denominator involving the disk velocity field ultimately reduces to $\sqrt{1 - w_{\rm z}^2}$, which is unity at line center and becomes infinite at the line wings. Obviously, the infinite emission at the extreme wings is not physical but arises as an artifact of treating a disk with zero thickness. Note that even though the specific flux blows up at the largest Doppler shifts, one can readily verify that the total line flux (alternatively, the line equivalent width) is indeed finite by integrating over all Doppler shifts to yield $F_\nu = \pi F_0\,[1 + 0.125E_1(1 - 3\cos^2 i)]$.

In the limit of pure isotropic scattering, the parameter E_1 is zero, giving $F_\nu/F_0 = (1 - w_{\rm z}^2)^{-1/2}$ which is the solution for an equatorial ring or disk that is in constant expansion or rotation. As expected, the profile is symmetrically double-horned and cannot be used to distinguish between expansion and rotation. With $E_1 \neq 0$ signifying anisotropic scattering, the respective profile shapes are no longer equivalent. To compare the two cases, a normalization is chosen to extract the underlining double-horned trend, namely

$$A \equiv \frac{1}{2}\,\sqrt{1 - w_z^2}\,\frac{F_\nu}{F_0}, \tag{12}$$

where the factor of 1/2 is included to cancel the factor of 2 that will appear in F_ν, since two radial spokes contribute to the emission at any given Doppler shift (see Fig. 2). The solution for rotation and expansion separately becomes

$$A_{\rm exp} \;=\; 1 - \frac{1}{4}E_1\,\left(1 - 3\sin^2 i\,w_{\rm z}^2\right), \tag{13}$$

$$A_{\rm rot} \;=\; 1 - \frac{1}{4}E_1\,\left[1 - 3\sin^2 i\,(1 - w_{\rm z}^2)\right]. \tag{14}$$

The only difference between the two expressions is the sign in the last term. The sign change results from the Doppler pattern for the rotation case being shifted 90° clockwise with that for expansion.

The functions $A_{\rm exp}$ and $A_{\rm rot}$ are plotted in Fig. 3a–d. The panels (a) and (c) are for expansion and (b) and (d) are for rotation. Panels (a) and (b) show curves with values of $E_1 = 0.0$, 0.25, 0.5, and 1.0 for a disk that is viewed ege-on. The $E_1 = 0.0$ case is the horizontal line, and curves with increasingly greater deviations from horizontal are for increasing values of E_1. For the case of expansion, the anisotropic scattering yields emission that is enhanced in the wings and depressed at line center. This is explained by realizing that light which is forward scattered, corresponding to maximal Doppler shifts, is brighter than light that scatters through a right angle, corresponding to line center with zero Doppler shift along the line-of-sight. For the rotation case, the trend is exactly opposite, because forward scattering now occurs at zero Doppler shift and right angle scattering corresponds to the line wings.

Notice also that all the curves in (a) and (b) intersect at a common point where $w_{\rm z}^2 = 1/3$ in the expansion case and $2/3$ in

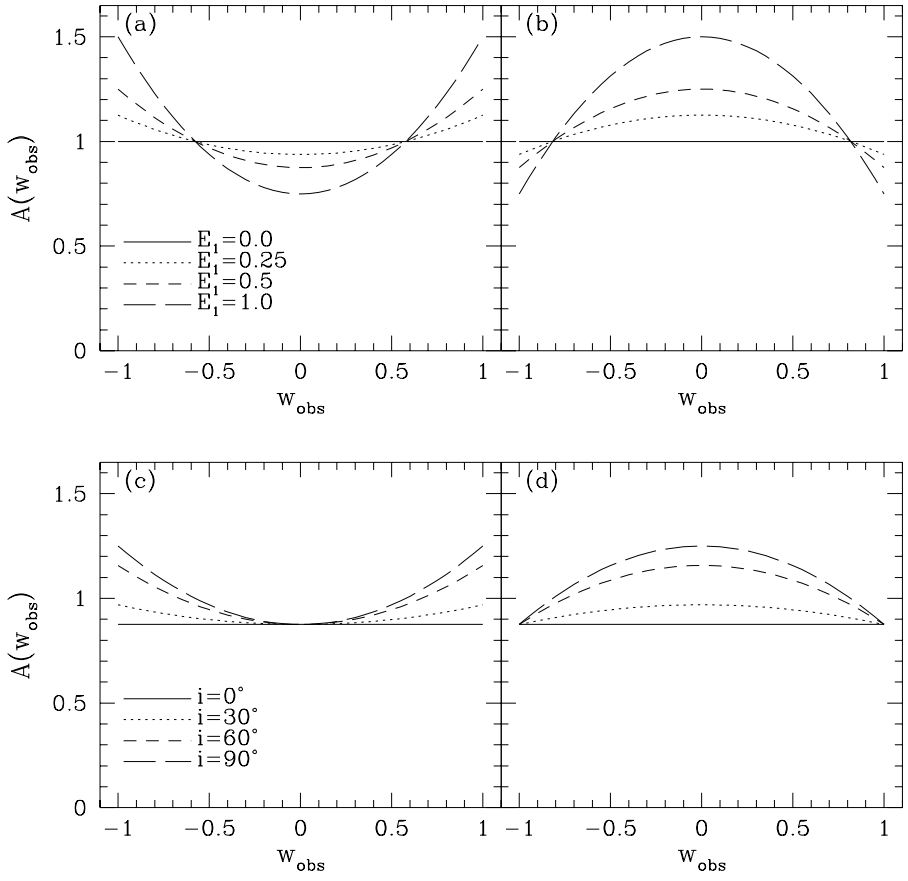

Fig. 3a–d. Resonance scattering line profiles for a planar equatorial disk illuminated by a central point source. The case of constant expansion is left in **a** and **c** whereas constant rotation is right in **b** and **d**. The two upper panels show A plotted against normalized Doppler shift for a disk viewed edge-on with $E_1 = 0.0, 0.25, 0.5$, and 1.0. The $E_1 = 0$ case is flat in both **a** and **b**, and curves that deviate more from a straight line have larger E_1 values. Similarly, **c** and **d** show curves for fixed $E_1 = 0.5$ but different viewing inclinations, ranging from $i = 0, 30, 60$, and 90 degrees. For these curves the flat one corresponds to a pole-on view.

the rotating case. In both cases the scattering angle corresponds to $\varphi = 54.7°$, known as the Van Vleck angle.

Panels (c) and (d) are for a fixed value of $E_1 = 0.5$ but different inclinations with $i = 0$, 30, 60, and 90 degrees. The pole-on case yields the horizontal line, and the curve with the greatest bow is edge-on. The pole-on perspective is a somewhat odd case to consider, because $\sin i = 0$, thus v_z is zero and F_0 becomes infinite. This mathematical difficulty arises from the assumption of a zero thickness disk, an assumption that is clearly breaking down near pole-on viewing perspectives. For a real disk of small opening angle, the emission will be strong but the profile will be narrow, at least Doppler broadened according to the temperature of the disk gas. Even so, the pole-on case is included here because the normalized profile does demonstrate how the anisotropic scattering reduces the amount of line emission along the pole for increasing values of E_1, a valid result that is attributable to this scattering geometry.

Eqs. (13) and (14) make a simple prediction about the line profiles of different E_1 values. The normalized difference profiles in the case of expansion is

$$A_{\rm exp}(E_1) - A_{\rm exp}(0) = -\frac{1}{4} E_1 \left(1 - 3\sin^2 i\, w_z^2\right), \qquad (15)$$

and that for rotation is

$$A_{\rm rot}(E_1) - A_{\rm rot}(0) = -\frac{1}{4} E_1 \left[1 - 3\sin^2 i\,(1 - w_z^2)\right]. \qquad (16)$$

The important result here is that the difference profiles for an expanding disk are parabolic up; those for a rotating disk are parabolic down. So the anisotropic scattering provides a straightforward signature of the disk velocity field.

Note also that the profile differencing allows for the inclination to be estimated. However, to do so requires that the parameters (e.g., Σ_0) making up the scaling constant F_0 be known. Profile ratios were also considered and give similar diagnostic signatures; however, the differencing of normalized profiles may provide a better diagnostic because typical profiles will be modified by photospheric and wind absorption and by occultation, so that differencing seems a more reasonable procedure for comparing lines of different E_1 values.

In this discussion the underlining disk model is obviously extremely simplified: optically thin, geometrically thin, neither accelerating for expansion nor Keplerian for rotation; yet, the *qualitative* trend predicted by the simple disk model should hold independent of these factors because the results of Eqs. (15) and (16) rely on the relation between the isovelocity zones and the scattering geometry. The isovelocity zones for realistic disk velocity distributions can deviate substantially from the simple spokes associated with constant expansion or rotation, but the extrema in Doppler shifts still correspond to roughly the same scattering geometries, and similar results are expected, as discussed in Sect. 2.2. In addition to realistic disk velocity fields, the star's finite size can also alter the profile shape. The follow-

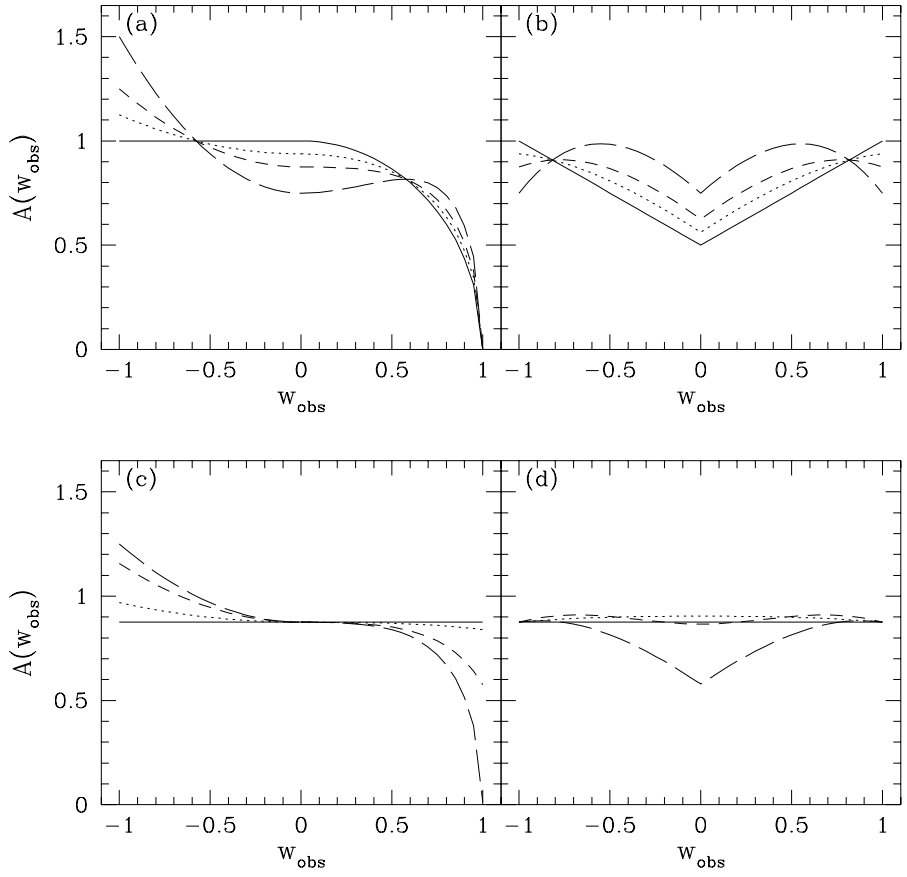

Fig. 4a–d. As in Fig. 3a–d but now taking the stellar occultation into account.

ing derivations explore the consequences of these *geometric* effects.

2.1.2. The effect of occultation

If the scattering region extends down to the stellar radius, then occultation cannot be ignored. The lower boundary to the integration over cylindrical radius in Eq. (10) is now a function of the Doppler shift in the profile and the viewing inclination. The problem is to determine where rays intersect the disk if tangent to the stellar photosphere and to relate that locus of points to the corresponding line-of-sight Doppler shifts. The geometrical solution has been discussed by Fox & Brown (1991) who derived

$$\varpi_0 = \left(1 - \sin^2 i \cos^2 \varphi\right)^{-1/2}, \tag{17}$$

which traces the projection of the stellar limb onto the disk. It is straightforward to relate ϖ_0 to w_z using Eq. (7) for the dependence of Doppler shift on $\varphi = \varphi_0$. In the case of constant expansion, $\varpi_0 = (1 - w_z^2 \sin^2 i)^{-1/2}$; for pure rotation the solution is $\varpi_0 = (\cos^2 i + w_z^2 \sin^2 i)^{-1/2}$.

To isolate the effects of occultation, a point source as in the previous section is again assumed to approximate the illumination of the scatterers. To derive the emission profile from the disk, the integral equation of (10) is used, with the limits of ϖ extending from ϖ_0 to ∞ instead of 1 to ∞ as for the point star case. For pure expansion the solution is

$$A_{\rm exp}(w_{\rm obs} > 0) \;=\; \varpi_0^{-1} \left\{ 1 - \frac{1}{4} E_1 \left(1 - 3 \sin^2 i \, w_z^2 \right) \right\}, \tag{18}$$

$$A_{\rm exp}(w_{\rm obs} \leq 0) \;=\; \left\{ 1 - \frac{1}{4} E_1 \left(1 - 3 \sin^2 i \, w_z^2 \right) \right\}, \tag{19}$$

where the second line is just the point source solution of the previous section which is accurate for the blueshifted frequencies that are unaffected by occultation. For pure rotation the expression is

$$A_{\rm rot} = \frac{1}{2} \left(1 + \varpi_0^{-1}\right) \left\{ 1 - \frac{1}{4} E_1 \left[1 - 3 \sin^2 i (1 - w_z^2) \right] \right\}. \tag{20}$$

Fig. 4a–d shows the striking difference between profiles of expanding disks as contrasted to ones that rotate when occultation is included. For expansion occultation has consequence for the redshifted emission only, with greatest effect at the extreme line wing where scattering material receding directly away from the observer suffers the greatest occultation. But for rotation the occultation blocks some light at all w_z, with greatest effect at line center where the isovelocity zone that contributes to the line emission at $w_z = 0$ is directly along the line-of-sight passing through the star.

Instead of elaborating on the difference profiles here, the consequences of finite star depolarization are first presented in the next section. The difference profiles are considered in the section following that takes account of all the finite star effects.

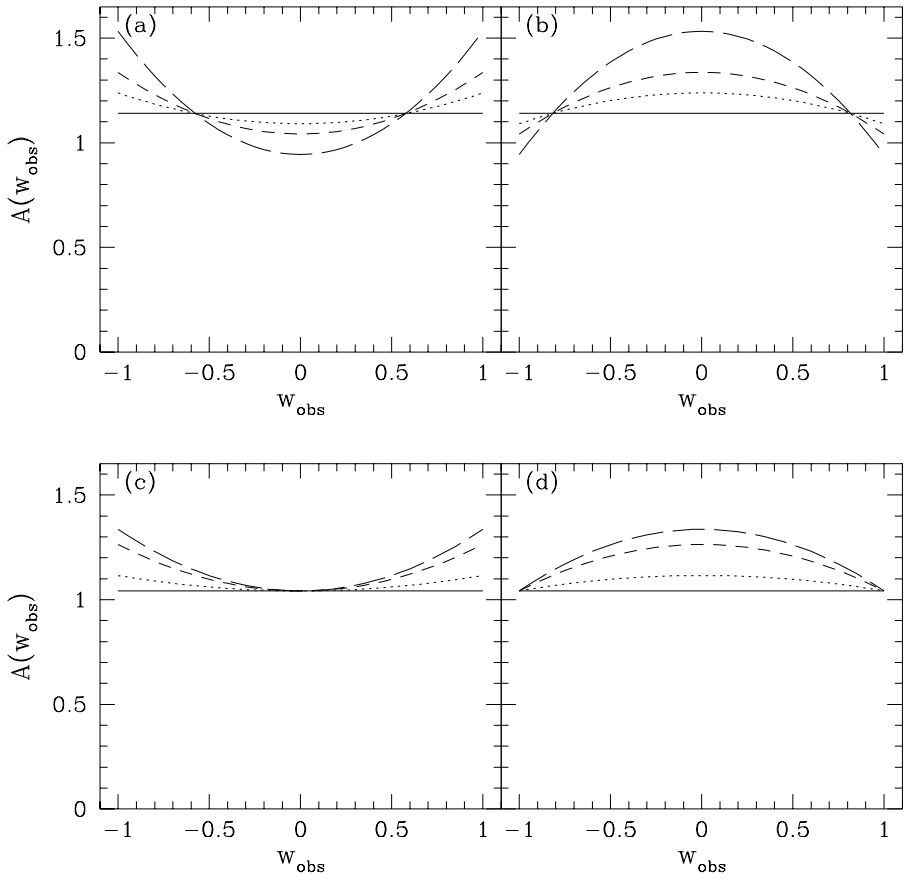

Fig. 5a–d. As in Fig. 3a–d but now taking the finite star depolarization into account.

2.1.3. The effect of finite star depolarization

Cassinelli et al. (1987) discussed how the continuum polarization arising from electron scattering can be reduced at small radii where the star cannot be treated as a point source. The reduction of polarization owes to the more nearly isotropic distribution of incident stellar light at the scatterer. This same effect holds for the case of resonance line scattering, since the anisotropic line effects derive from dipole scattering just as for free electrons. Following Cassinelli et al., the depolarization effect (or alternatively the isotropizing effect) of the finite star is implicit in the appearance of $\tilde{J}_\nu$ and $\tilde{K}_\nu$ of Eq. (10).

For the case of a uniformly bright stellar disk, the familiar forms of $\tilde{J}_\nu = 2(1-\cos\theta_*)$ and $\tilde{K}_\nu = \frac{2}{3}(1-\cos^3\vartheta_*)$ are found, where the geometrical factor $\cos\theta_* = \sqrt{1-\varpi^{-2}}$. Ignoring the occultation, the solution to the integral expression (5) is

$$A_{\rm exp} \;=\; (\pi-2)\left\{1-\frac{\pi/16}{\pi-2}E_1\left(1-3\sin^2 i\; w_{\rm z}^2\right)\right\}, \quad (21)$$

$$A_{\rm rot} \;=\; (\pi-2)\left\{1-\frac{\pi/16}{\pi-2}E_1\left[1-3\sin^2 i\,(1-w_{\rm z}^2)\right]\right\} \quad (22)$$

Fig. 5a–d shows these functions in the same format as previous figures. With the finite depolarization effect, the functional dependence on $w_{\rm z}$ is preserved as in the point star case, only some coefficients are altered. There is now a leading coefficient of 1.14. The numerical coefficient of the E_1 term is no longer 0.25 but 0.172, a decrease of about 30%. As can be seen from Fig. 5a–d, this decrease results in a reduced variation between curves with different values of E_1 and viewing inclinations. The combined effects of stellar occultation and finite star depolarization are derived next.

2.1.4. The combined finite star case

The profile shapes with both occultation and finite star depolarization are determined from Eq. (10) using $\tilde{J}_\nu$ and $\tilde{K}_\nu$ from the previous section with the appropriate integral limits for occultation. For constant expansion recall that $A_{\rm exp}(w_{\rm obs}\le 0)$ is not affected by the occultation so that expression (21) applies at the blueshifted velocities. The redshifted profile is modified by the occultation and is given by

$$A_{\rm exp}(w_{\rm obs}\ge 0) \;=\; 2\left\{\sin^{-1}\varpi_0^{-1}+\sqrt{\varpi_0^2-1}-\varpi_0 - \frac{1}{16}E_1\left(1-3\sin^2 i\, w_{\rm z}^2\right)\left(\sin^{-1}\varpi_0^{-1}+\varpi_0^{-1}\sqrt{1-\varpi_0^{-2}}\right)\right\}. \quad (23)$$

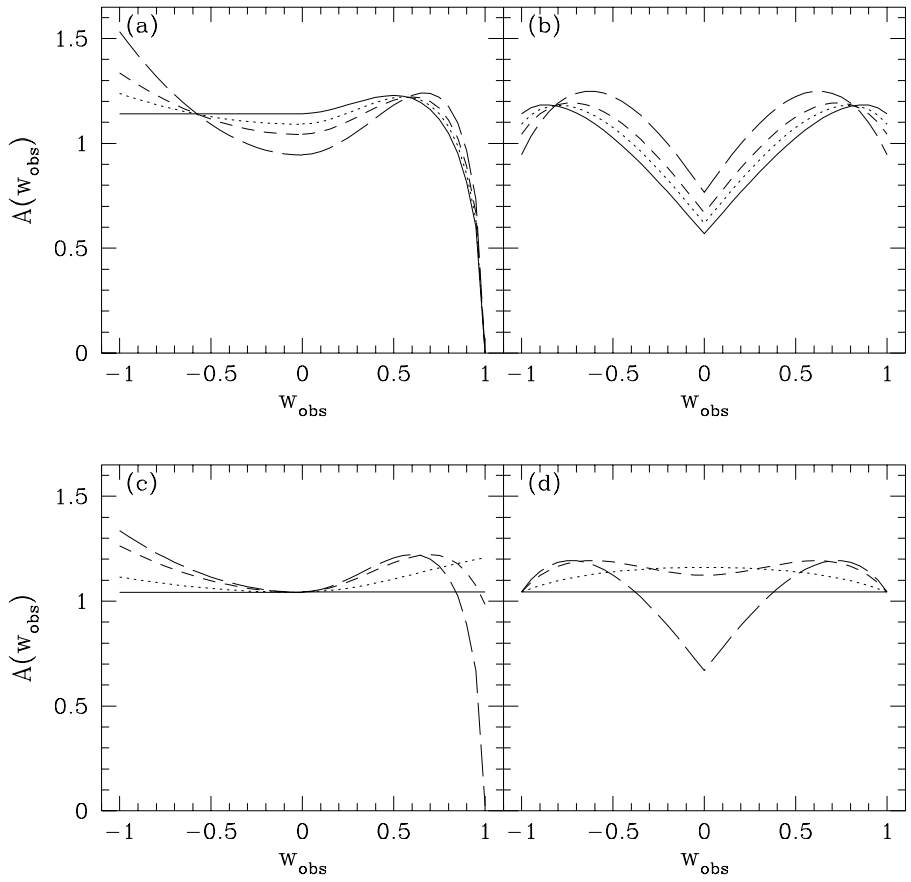

Fig. 6a–d. As in Fig. 3a–d but now including the effects of both occultation and finite star depolarization.

Note that in the pole-on case, ϖ_0 reduces to unity, and Eq. (21) for the line emission with finite star depolarization is recovered. For constant rotation the profile is given by

$$A_{\rm rot} = \frac{\pi}{2} - 1 + \sin^{-1}\varpi_0^{-1} + \sqrt{\varpi_0^2 - 1} - \varpi_0 - \frac{1}{16} E_1 \left[1 - 3\sin^2 i\,(1 - w_{\rm z}^2)\right] \left(\frac{\pi}{2} + \sin^{-1}\varpi_0^{-1} + \varpi_0^{-1}\sqrt{1 - \varpi_0^{-2}}\right). \quad (24)$$

Again for a pole-on perspective, there is no occultation, and Eq. (24) reduces to that of (22).

Fig. 6a–d plots $A(w_{\rm obs})$ in both cases. The concavity of the two respective cases remains a distinct signature of the velocity field. Difference profiles $A(E_1) - A(0)$ are shown in Fig. 7a–d. It is the difference profiles that will serve as the best diagnostic of the disk velocity field. Bearing in mind that the normalized profiles A have values of order unity at most values of $w_{\rm obs}$, the fact that the difference profiles can have values as large as 0.1 and 0.2 in some cases indicates that the anisotropic scattering modifies the profiles at the 10 and 20% level.

Unfortunately, the concavity of the difference profiles for the expanding disk case is actually *concave down* in the far red wing, owing to the effects of occultation. The change in concavity would appear to seriously compromise the diagnostic utility of these results; however, the difference profile at the redshifted velocities has a turnover where it becomes concave up closer toward line center, whereas the profiles for rotating disks are concave down everywhere.

2.2. Line profiles from disks in linear expansion or Keplerian rotation

Having derived analytic results for simplified cases to highlight the consequences of anisotropic scattering in disks and the various finite star effects, line profiles for more realistic disk velocity fields are derived in this section. Several assumptions remain, such as the lines being optically thin.

The Appendix details some technical aspects of the profile calculations; however, a few comments are made here about the effects of absorption before proceeding to a discussion of the results. First, the value of ϖ_0 used to determine the stellar occultation is also relevant to the absorption. For occultation ϖ_0 indicates where the projected limb of the star falls onto the circumstellar disk; for absorption its value indicates the extent of the disk on the near side that shadows the lower facing stellar hemisphere. Consequently, absorption will be less significant for more pole-on viewing perspectives since ϖ_0 tends toward unity.

Second, where the absorption occurs in the profile in very different for expansion than for rotation. In the former the absorption is only in the blueshifted wing. As discussed in paper I, this fact is quite convenient allowing to ignore the absorption

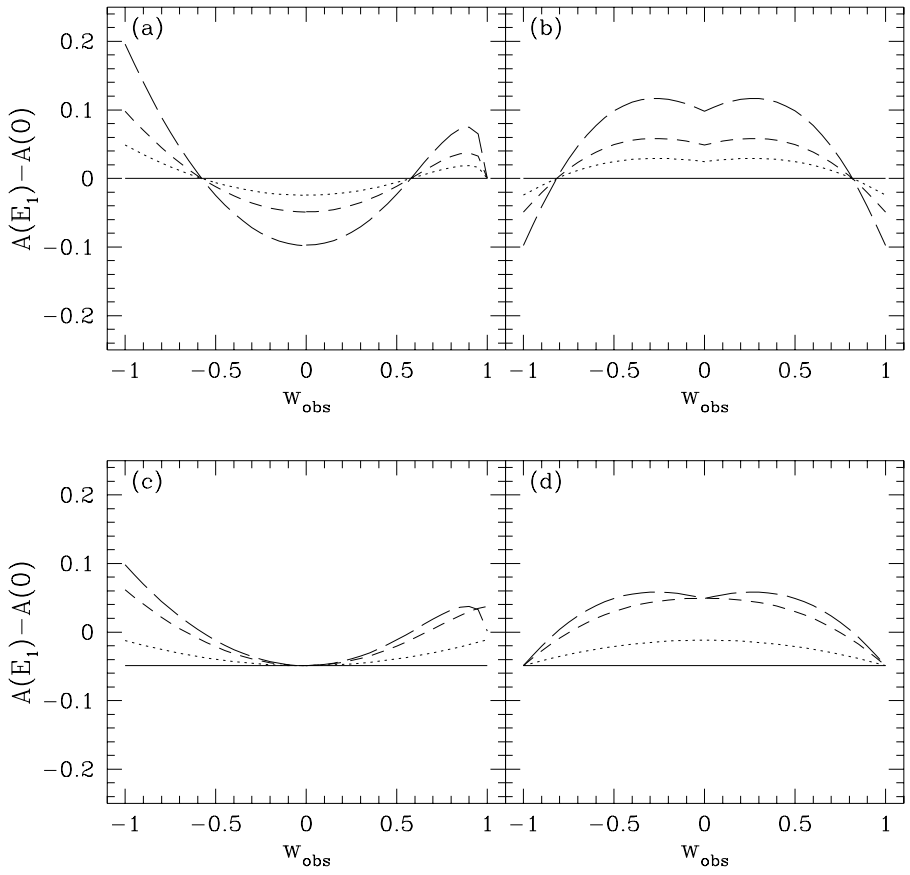

Fig. 7a–d. Difference profiles for the E_1 and inclination values of the previous figures. Note the concavity of the difference profiles for expansion (left) remain distinct compared to those for rotation (right). Bearing in mind that the normalized profiles A are themselves of order unity, the difference profiles show up to 20% level variations across the range of Doppler shifts between the lines of $E_1 = 0$ and $E_1 = 1$.

and focus on the redshifted profile where only the geometric effect of occultation is concerned. However, unlike expansion, absorption generally modifies the *entire* profile in the case of rotation. Nevertheless, it can be concluded that for both expansion and rotation, absorption will tend to have greatest effect near line center, with diminishing significance toward the line wings. Note that the continuum flux can be reduced by at most 50%, because the disk can only attenuate the lower stellar hemisphere.

2.2.1. The case of linear expansion

Line profiles have been computed for a disk that expands linearly as

$$v_{\rm R} = v_\infty \, \frac{\varpi}{\varpi_{\rm max}}, \tag{25}$$

where $\varpi_{\rm max}$ represents a transition from linear expansion to constant expansion. Using this velocity parametrization, the isovelocity zones reduce to lines of constant $z = x_* \sin i$ in the region of acceleration. The surface number density of the disk becomes

$$\Sigma(\varpi) = \Sigma_0 \, \frac{\varpi_{\rm max}}{\varpi^2}. \tag{26}$$

Fig. 8 shows line profiles for linear expansion using a value of $\varpi_{\rm max} = 10$, beyond which the contribution to the emission by the constant expansion flow is simply ignored. Results are given for three different viewing inclinations of $30°$, $60°$, and $89°$ from top to bottom. The latter is chosen because a planar disk viewed perfectly edge-on degenerates to a line as projected against the plane of the sky, an artifact of the disk having zero thickness. The left column shows the profiles with solid for $E_1 = 0$ and dashed for $E_1 = 1$, the two extreme cases. Recall that F_ν is the flux of line emission only, hence the vertical axis is $(F_{\rm c} + F_\nu)/F_{\rm c} = 1 + F_\nu/F_{\rm c}$, for $F_{\rm c}$ the stellar continuum flux outside the line frequencies. The right column shows the difference profiles $\Delta(F_\nu/F_{\rm c})$.

There are several points to note in the results of Fig. 8. (1) The emission mostly appears at low observed Doppler shifts, a consequence of the density decreasing as ϖ^{-2}. (2) The emission generally shows a double spike; however, the spike on the redshifted side is largely absent owing to the occultation. (3) The difference profile is distinctly concave up and negative near line center but is zero in the wings. For more pole-on inclinations, the profile is reasonably symmetric about line center indicating that absorption and occultation do little to contaminate the difference profile, as predicted. For more edge-on inclinations, the effects of absorption and occultation are more severe as anticipated, although the signature of positive concavity is still present near line center. (4) The overall amplitude of the difference profiles is a small fraction of the line emission *above* the continuum (which is the relevant quantity for comparison), amounting to a 10% level variation near line center. This is somewhat reduced from the results of the previous sections and reflects the fact that

scattering in the isovelocity zones now samples a range of scattering angles, in contrast to the constant expansion case where the scattering angle was fixed along any given radial spoke.

The fact that the greatest variation appears near line center suggests that the interpretation of difference profiles from two lines with different E_1 values may be complicated by the presence of photospheric absorption. The significance of the photospheric contamination depends on the relative widths of the signature for anisotropic scattering versus that of the absorption line. Fig. 8 indicates that the anisotropic effects are most prominent for $w_{\rm obs}$ within about ± 0.25 of line center. Most hot star winds have terminal speeds around 1000 $\rm km\ s^{-1}$ or higher; however, the disks of Be and B[e] stars appear to have much slower flows of around 100 $\rm km\ s^{-1}$ (e.g., Zickgraf 1986). The signature of anisotropic scattering would therefore be in the range $\pm 25\ \rm km\ s^{-1}$ of line center, a value not too much in excess of the thermal broadening expected for the photospheric lines. It would appear difficult to observe the effects of anisotropic scattering in the difference profiles, except in the following cases. (a) Some disks may have more rapid terminal speeds so that the signature of anisotropic scattering is significantly wider than the thermal broadening. (b) The line of interest is formed at large radius lying outside the acceleration region (e.g., owing to the ionization distribution), in which case the line will be broadened to the full extent of the disk terminal speed. Or, (c) multiplet lines are used, in which case the photospheric absorption in the different components comes from the same atmospheric layers and may therefore be easier to correct in the difference profiles. The use of multiplet lines is discussed further in Sect. 3.

2.2.2. The case of Keplerian rotation

The velocity field used for a rotating disk is the Keplerian prescription with

$$v_\varphi = v_{\rm rot}\, \varpi^{-1/2}, \tag{27}$$

where $v_{\rm rot}$ is the equatorial rotation speed. In the case of linear expansion, the isovelocity zones reduce to lines of constant z, but for rotation the topology of the zones is more complicated. A plot of the topology is given in Fig. 2 of Wood & Brown (1994a). Emission at line center emerges along a ray that extends from the observer and passes through the center of the star. The extreme wings in $w_{\rm obs}$ correspond to points at the limb of the star in the plane of the sky. The other isovelocity zones are shaped like "lobes" that are axisymmetric about y_*.

In the absence of radial flow, more freedom is allowed in choosing the density distribution of the disk. The disk density is here assumed to decrease with radius and is parametrized as

$$\Sigma = \Sigma_0\, \varpi^{-q}, \tag{28}$$

with q positive. So as to make comparison with the expansion case more direct, line profiles have been computed using $q = 2$ (c.f, Eq. [26]). The scaling parameter for the line emission from the disk is also chosen to be the same for the Keplerian case as for the linear expansion case.

Line profiles from a Keplerian disk are shown in Fig. 9, in the same format as Fig. 8 for the expanding case. The profiles from the rotating disk look radically different from those of an expanding disk: the lines are double-peaked but much broader and the anisotropic effects are considerably more prominent. The difference profiles shown in the right column are distinctly concave down, exactly opposite to the case of expansion, and the amplitude is a much more significant fraction of the line emission *above* the continuum. In regard to the latter point, it should be noted that absorption and occultation are greatest near line center, so that the apparent line emission is significantly reduced in the vicinity of line center.

One expects $v_{\rm max}$ in a Keplerian disk to be limited by the critical rotation speed of break-up of the star, around 500 $\rm km\ s^{-1}$ for hot stars. Typical values of $v_{\rm max}$ around a few hundred $\rm km\ s^{-1}$ or less can therefore be expected of Keplerian disks, which is of the same order as the slowly expanding disks. Consequently, the width of the emission profile is not sufficient to distinguish between expanding and rotating disks, so that the effects of anisotropic resonance scattering could prove to be an important diagnostic of the disk flow properties.

3. Discussion

This paper presents a first step in exploring the consequences of anisotropic resonance line scattering in circumstellar disks for diagnosing expansion versus rotation. The motivation for considering disks relates to the conclusion from paper I that anisotropic line scattering has little effect on emission profiles from spherical winds owing largely to the consequences of stellar occultation, but may be of greater importance for aspherical envelopes where the significance of occultation is inclination dependent. Although several simplifications were used in the derivations of this work, the results give clear-cut signatures of the disk velocity field when those simplifications apply and qualitative insight into more general cases.

There are several practical considerations that should be noted in applying the results of this paper to observations.

1. Some remarks in addition to those previously mentioned on photospheric absorption are needed. For a rotating star with a disk that is fed by the star itself, the disk will not rotate faster than the central star, hence any photospheric absorption component from the star will modify the entire profile shape. However, if the disk is one of accretion (e.g., onto a white dwarf star), some parts of the inner disk can actually rotate faster than the star, and the photospheric contribution to the line could be isolated to the line core.
2. The diagnostic scheme suggested here has been to difference profiles with various E_1 values. Tables for computing E_1 values for specific line transitions can be found in App. A of Jeffery (1989). Values of E_1 for several common resonance lines of astrophysical interest were listed in Tab. 1 of paper I. Note that strong doublets from the ground state of Lithium-like atoms have $E_1 = 0.5$ for the short wavelength component and $E_1 = 0.0$ for the long wavelength

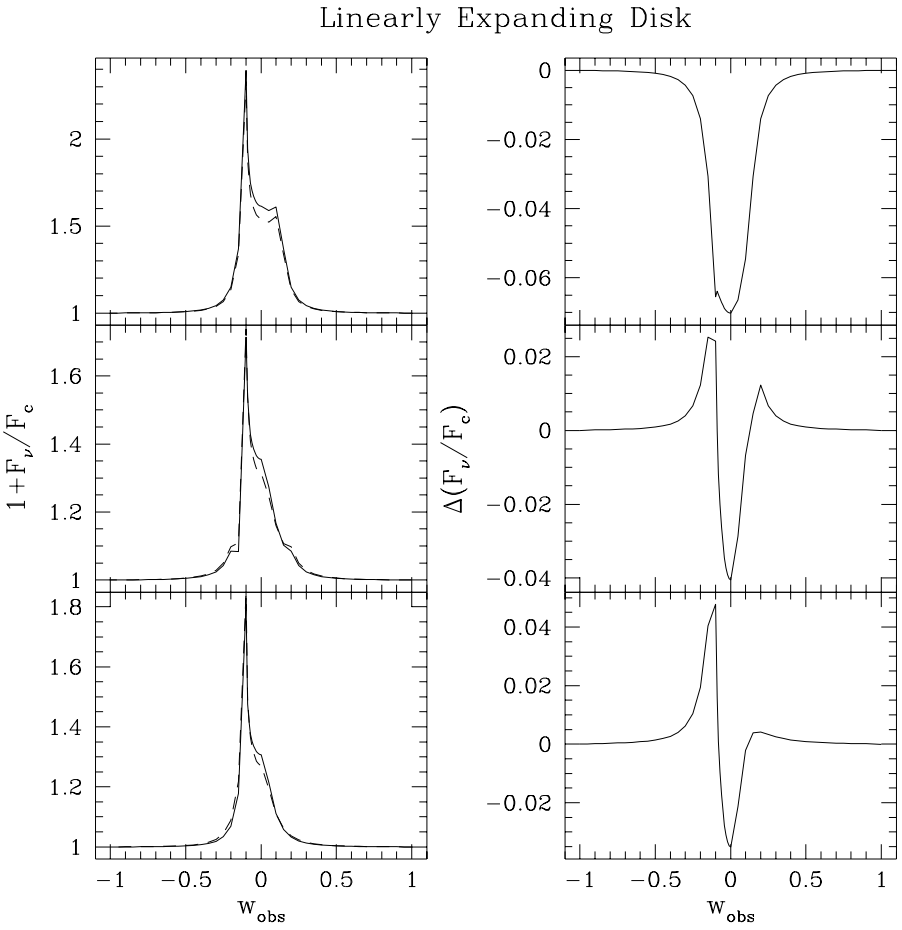

Fig. 8. Line profiles from a disk in linear radial expansion. Left shows the profiles for viewing inclinations of $30°$, $60°$, and $89°$ from top to bottom. Solid is for isotropic $E_1 = 0$ scattering and dashed for dipole $E_1 = 1$ scattering. Right shows the difference profiles. Relative to the emission *above* the continuum, the anisotropic scattering produces at most 10% level differences between the two cases.

component, immediately providing two lines for profile differencing (if unblended) that (a) are very close in wavelength and (b) form in the same spatial region of the envelope.

3. Of course, care must be taken in the line selection, making sure the chosen lines are indeed formed in the disk and not outside it. Although the focus of this work has been on isolated equatorial disks, real stars experience mass loss at all latitudes, so that an observed spectrum may contain lines that arise from different parts of the flow, both in radius and latitude. A good example is the B[e] stars that exhibit a range of ionization states in their spectra. It is believed that the narrower, low ionization state lines (e.g., FeII) form in an equatorial disk but the broader, higher ionization states (e.g., CIV) occur in a fast polar wind (Zickgraf et al. 1986). In this example the line width is a reasonably clear indicator of those lines that are from the disk.
4. Also related to line selection, the results of this paper have assumed optically thin line emission. The effects of multiple scattering will be to isotropize the emergent light. In the same way that polarization is reduced by multiple scattering, so resonance lines of different E_1 values will produce increasingly similar profile shapes for increasing line optical depths (all else being equal), because the profile effects arising from the anisotropy are lost after a few scatterings. As multiple scattering becomes important, it is the emission emerging from the inner regions where the envelope is presumably densest that will be affected first. Thus, multiple scattering will have chief importance at frequencies near line center for expanding disks and at all line frequencies for rotating disks.
5. This paper has concentrated on only expansion or rotation, but not the combination. For disks with both expansion and rotation of comparable speeds, the diagnostic value of anisotropic line scattering for probing the disk velocity field may be reduced. However, comparison of Figs. 5, 7, and 9 of Wood et al. (1993) for disks with just expansion, just rotation, and both together suggests that at small radii the location of the isovelocity zones in the combined case is similar to that for pure rotation, with the pattern being slightly shifted counterclockwise. Since the bulk of line emission arises from the densest inner regions, the results derived here for a pure Keplerian disk may have some relevance to disks that are expanding and rotating, especially if the initial speed of expansion is small compared to $v_{\rm rot}$.

There are other related means using the properties of anisotropic line scattering that may be employed to infer the structure of circumstellar envelopes, be they jets, disks, or spheres. The first regards intrinsic line polarization. For $E_1 \neq 0$, the anisotropic scattering produces polarized light line emission for aspherical envelopes. In fact, the calculation of *optically*

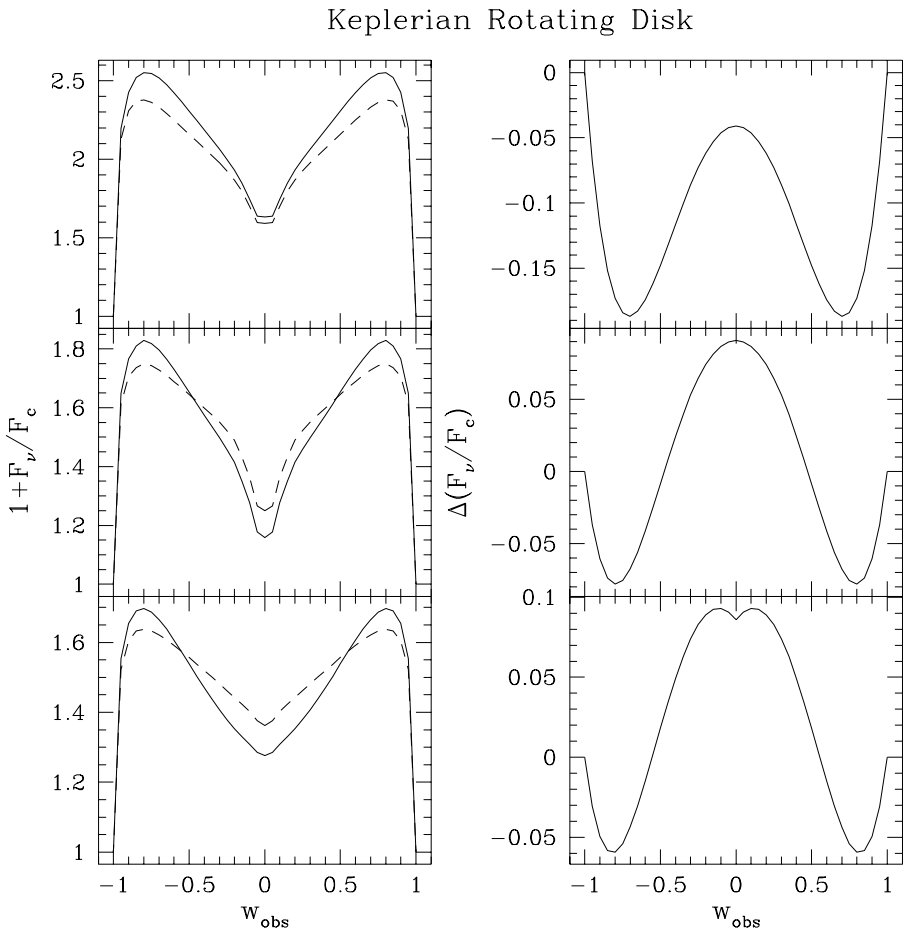

Fig. 9. Shown are line profiles from a Keplerian disk on left with solid for isotropic scattering $E_1 = 0$ and dashed for dipole scattering $E_1 = 1$. Right shows the difference profiles. From top to bottom, the viewing inclinations are 30°, 60°, and 89°. The downward concavity of the difference profiles over most observed Doppler shifts is a clear signature of the rotation.

thin polarized lines bears strong resemblance to the methods of Brown & McLean (1979) and Cassinelli et al. (1987), except that the volume integrals are confined to isovelocity zones in contrast to the entire scattering region. The work of Jeffery (1989, 1990) illustrates the computation of polarized line profiles from resonance line scattering with application to the expanding envelopes of SNe.

It is also interesting to consider line formation in media where relativistic effects are important, for example in flows that travel at relativistic speeds or scattering regions in the vicinity of compact objects. The line profile shapes can be dramatically altered from what is produced in non-relativistic envelopes (e.g., Hutsemékers 1990; Bao et al. 1994). The isovelocity zones are significantly distorted relative to the non-relativistic case, hence the scattering geometry is also significantly modified, so that anisotropic line scattering which has not been considered in previous calculations might be important.

A second relativistic effect that could prove to be a valuable diagnostic of velocity fields in circumstellar envelopes is that of microlensing. As a hypothetical case, consider a planar disk that is viewed nearly edge-on. If this disk is expanding and microlensed by some intervening compact object, the entire profile should be affected symmetrically about line center, since a ray joining the observer and the lens and passes through the disk samples the full range of Doppler shifts. Thus, the entire profile is amplified symmetrically about line center. In contrast for a rotating disk, the profile should respond quite asymmetrically, because unlike the expanding case, all the Doppler motions that are redshifted appear on one side of the disk as seen by the observer, and all those blueshifted appear on the opposite side. Thus, a ray passing through the disk along the line-of-sight joining the observer and lens *does not* sample all Doppler shifts. Qualitatively, as the lens moves across the disk, the amplification of the profile will start at one wing and progressively move across the profile to the opposite wing.

Of equal interest are the relative responses of the line emission and the continuum emission. For example, if the continuum arises solely from the star, amplification should first occur in the line profile owing to the much greater extension of the line emitting region. Contrastly, for wavelengths where the continuum emission arises from the wind itself (as occurs in dense winds at infrared and radio wavelengths), both the line and continuum emission become amplified more or less contemporaneously.

Detailed modeling must be done to confirm these various predictions. The statistical expectation of microlensing events of mass losing hot stars may be rather low (Coleman 1998), but the diagnostic value afforded by any such events would be exceedingly great. The topic therefore warrants continued study.

Acknowledgements. I want to thank Drs D. Clarke and M. Hendry for several helpful discussions. I also thank an anonymous referee for

suggestions leading to substantial revisions and improvements of the paper. This research was conducted under funding from a UK PPARC Rolling Grant.

Appendix A: optically thin line profiles from planar disks including the effects of absorption

This appendix details some of the technical aspects associated with the calculation of the line profiles in Sect. 2.2 for realistic disk velocity fields. The calculation of the emission from the disk is based on Eqs. (7) for the location of the isovelocity zones and (10) for the flux of emission from the disk, including the effects of occultation and finite star depolarization.

The major new ingredient in the computations is the consideration of absorption. The amount of stellar continuum radiation observed in a small interval of frequency $\nu_z \pm \Delta\nu_z$ within the broadened line depends on two things: the fraction of the star's surface that is covered by disk material and the optical depth of that material. In regard to the former, the observed flux of continuum emission $F_c(\nu_z)$ consists of a fraction that is direct, or unattenuated, and a fraction that is attenuated. The attenuating material is located on the near side of the star and covers an area in the disk that is traced by $\varpi_0(\varphi)$ given of Eq. (17). This attenuating regions covers only the lower facing stellar hemisphere. However, for a small interval of frequency in the line, only a relatively fraction of that covering area contributes to the absorption.

The expression for the continuum emission is

$$\frac{F_c(\nu_z)}{F_*(\nu_0)} =$$

$$\frac{A_* - A_\perp(\nu_z)}{A_*} + \frac{A_\perp(\nu_z)}{A_*}\left(\frac{1}{A(\nu_z)}\int_{\nu_z} e^{-\tau_\nu}\, dA\right), \qquad \text{(A1)}$$

where $F_*(\nu_0) = L_*(\nu_0)/4\pi D^2$ is the stellar continuum flux at the wavelength of the line and is assumed constant over the range of line frequencies, $A_* = \pi R_*^2$ is the projected area of the star, $A(\nu_z)$ is the geometrical area in the disk (i.e., as viewed pole-on) presented by the absorbing material with opacity in the interval $\nu_z \pm \Delta\nu_z$, $A_\perp(\nu_z)$ is the projection of that area along the line-of-sight and is equal to $A(\nu_z)\cos i$, and τ_ν is the optical depth. Note that $F_c(\nu_z)/F_*(\nu_0)$ can never fall below 0.5 since the disk can at most cover half of the projected stellar surface.

The optical depth is given by

$$\tau_\nu = \int \Sigma\,\sigma_l\,\delta(\nu_{\rm obs} - \nu_z)\,dz = \Sigma\,\sigma_l\left|\frac{d\nu_z}{dz}\right|^{-1}_{z_0}, \qquad \text{(A2)}$$

where z_0 corresponds to a point in the disk where $\nu_{\rm obs} - \nu_z = 0$. An expression for the optical depth can be derived from (A2) for any given disk velocity field. The optical depth reduces to $\tau_\nu = \tau_0\, f(\varpi, \varphi)$, where τ_0 consists of scaling parameters such as Σ_0 and σ_l, and $f(\varpi, \varphi)$ is some function of position in the disk, the specifics of which depend on the particular velocity law. The point here is that the parameters included in τ_0 also appear in the scaling constant F_0 associated with the line emission from the disk. This is a natural consequence of the optically thin assumption. Consequently, the amount of emission and the degree of absorption are not independent but are coupled through the parameters common to τ_0. For the profile calculations of Sect. 2.2, it was noted that F_0 was chosen to be the same in both the linear expansion and Keplerian rotation cases. This choice effectively determines the ratio of τ_0 for expansion to that for rotation, which is of order unity. Absorption does not generally modifythe observed emission profile significantly (except near line center), because even if $e^{-\tau_\nu}$ tends toward zero, the coverage of the stellar surface presented by the disk for a given frequency interval in the line is typically a small fraction of πR_*^2.

References

Adams, F. C., Lada, C. J., Shu, F. H., 1987, ApJ 312, 788
Bao, G., Hadrava, P., Østgaard, E., 1994, ApJ 435, 55
Bjorkman, J. E., Bjorkman, K. S., 1994, ApJ 436, 818
Brown, J. C., McLean, S., 1977, A&A 57, 141
Brown, J. C., Fox, G. K., 1989, ApJ 347, 468
Brown, J. C., Wood, K., 1994, A&A 290, 634
Caroff, L. J., Noerdlinger, P. D., Scargle, J. D., 1972, ApJ 176, 439
Cassinelli, J. P., Nordsieck, K. H., Murison, M. A., 1987, ApJ 290, 302
Chandrasekhar, S., 1960, Radiative Transfer (New York: Dover)
Coleman, I. 1998, Ph.D. Thesis, Univ. Glasgow
Fox, G. K., 1991, ApJ 379, 663
Fox, G. K., Brown, J. C., 1991, ApJ 375, 300
Frank, A., Mellema, G., 1994, ApJ 430, 800
Hamilton, D. R., 1947, ApJ 106, 457
Hutsemékers, D., 1990, ApJ 361, 367
Ignace, R., 1998, A&A, 332, 686
Ignace, R., Nordsieck, K. N., Cassinelli, J. P., 1997, ApJ 486, 550
Jeffery, D. J., 1989, ApJS 71, 951
Jeffery, D. J., 1990, ApJ 352, 267
Kastner, J. H., Mazzali, P. A., 1989, A&A 210, 295
Kenyon, S. J., Hartmann, L., 1987, ApJ 323, 714
McKenna, S. J., 1984, Ap&SS 106, 283
McKenna, S. J., 1985, Ap&SS 108, 31
McLean, I. S., 1979, MNRAS 186, 265
Menzel D. H., 1929, PASP 41, 344
Mihalas, D., 1978, Stellar Atmospheres (Freeman: New York)
Nota, A., Livio, M., Clampin, M., Schulte-Ladbeck, R., 1995, ApJ 448, 788
Poeckert, R., Marlborough, J. M., 1978, ApJ 220, 940
Porter, J. M., 1997, A&A 324, 597
Quirrenbach, A., Buscher, D. F., Mozurkewich, D., A., Hummel, C. A., Armstrong, J. T., 1994, A&A 283, L13
Quirrenbach, A., Bjorkman, K. S., Bjorkman, J. E., et al., 1997, ApJ 479, 477
Stenflo, J. O., 1994, Solar Magnetic Fields (Dordrecht: Kluwer)
Struve, O., 1931, ApJ 73, 94
Waters, L., B., F., M., 1986, A&A 162, 121
Wood, K., Brown, J. C., Fox, G. K., 1993, A&A 271, 492
Wood, K., Brown, J. C., 1994a, A&A 285, 220
Wood, K., Brown, J. C., 1994b, A&A 291, 202
Wood, K., Bjorkman, K. S., Bjorkman, J. E., 1997, ApJ 477, 926
Zickgraf, F.-J., Wolf, B., Stahl, O., Leitherer, C., Klare, G., 1985, A&A 143, 421
Zickgraf, F.-J., Wolf, B., Stahl, O., Leitherer, C., Appenzeller, I., 1986, A&A 163, 119